A98-31599

ICAS-98-4,6,4

CONTROL SURFACE EFFECTIVENESS IN THE TRANSONIC REGIME

*F. Eastep**
University of Dayton
Dayton, OH, USA

*G. Andersen***, *P. Beran*†, *R. Kolonay*‡
Air Force Research Laboratory
Wright Patterson AFB, OH, USA

Abstract

This paper investigates control surface effectiveness in the transonic flight regime. Linear and nonlinear rigid and aeroelastic analyses are performed while including the effects of flow viscosity with an interactive boundary layer in the prediction of this aeroelastic parameter. Transonic small disturbance theory is employed in the analysis of a typical fighter type wing to study the interactions among control surface deflections, structural flexibility, and embedded shocks in a flow field where a viscous boundary layer exists. Pressure distributions on the wing are examined and control surface reversal calculations are presented. These results are discussed based on the predictions of the pressure coefficients generated by the solution of the transonic small disturbance equation. A limited number of Euler computational fluid dynamic solutions are presented for purposes of comparison of transonic small disturbance results with a higher order CFD code. Generalizations are offered concerning the effects of including viscosity in the prediction of steady aeroelastic phenomena in the transonic flight regime. The adequacy of using transonic small disturbance theory in the prediction of transonic airloads as compared to Euler CFD analyses is considered. Finally, the consequences of these findings on the preliminary design of aircraft structures are discussed.

Introduction

In order to perform structural design of flight vehicles, efficient and accurate maneuver loads predictions are required. Currently, there are many well established techniques available to determine steady aerodynamic loads and static aeroelastic responses in subsonic and supersonic flight. These methods are also often used in the transonic region. Since these methods are based on linear aerodynamic theory they are efficient but not considered accurate in this regime. The transonic flow condition is a mixture of subsonic and supersonic flow with embedded shocks; therefore, to accurately describe the transonic flow field, nonlinear partial differential equations must be solved.

Until recently, little effort has been expended to include nonlinear aerodynamic loads in the preliminary structural design environment due to the large computational cost associated with the solution of the nonlinear equations. The inclusion of viscous effects demands even more resources. However, with advances in nonlinear aerodynamic flow solvers and computer hardware, nonlinear airloads including viscous effects are now available at computational costs that make the problem tractable.

The intent of this research is to develop an efficient and accurate analysis that is capable of determining the aeroelastic response, including viscous effects, of a lifting surface with an articulated control surface in transonic flow. This method is then applied in the analysis of a simple fighter type wing to determine the significance of including viscosity in the analysis. Of particular interest is the rolling performance of a lifting surface in transonic flow. This study investigates the impact of including flow viscosity, aerodynamic

*Professor, Associate Fellow AIAA
**Aerospace Engineer, Capt. USAF, Member AIAA
†Aerospace Engineer, Senior Member AIAA
‡Aerospace Engineer, Member AIAA

nonlinearities, and structural flexibility in determining the control surface reversal dynamic pressures as compared to those found using a inviscid analysis in the transonic regime.

Background

Aeroelastic analysis of flexible aircraft structures in the transonic flight regime is a relatively recent endeavor. In the late '80s, research was conducted in the prediction of steady and unsteady airloads in the transonic region through the use of classical transonic small disturbance theory, and by employing the transonic full-potential equation.[1-2] Although both of these efforts included the effects of articulated control surfaces in the analysis, the effects of structural flexibility were not taken into account.

Currently, there is considerable interest in the United States Air Force in employing light weight reduced stiffness wing structures to effect maneuver performance. A rigid analysis is not sufficient in cases where a flexible structure deforms under the generated airloads. This issue was addressed under an Air Force contract with Rockwell International.[3] The study considered the effects of structural flexibility under the influence of airloads created by a deflected control surface. Degradation of rolling moment with increased dynamic pressure was shown for a limited range of Mach numbers. However, an in-depth investigation into the effect of varying Mach number and the interaction between shocks and control surfaces was not undertaken.

In 1991, transonic small disturbance theory was utilized to predict dynamic and steady aeroelastic phenomena concerning the F-15 and F/A-18 aircraft.[4] Although rolling moment coefficients were not directly observed, prediction of control surface reversal dynamic pressure was offered at a single Mach number through examination of the behavior of the computed lift coefficient for a lifting surface.

More recently, a study was undertaken which focused on a detailed examination of aeroelastic effects due to control surface deflections in transonic flow.[5] Emphasis was placed on accurate prediction of pressure distributions and steady aeroelastic phenomena. Rolling moments and control surface reversal points were examined as the Mach number was varied from subsonic to supersonic values. It was discovered that inclusion of nonlinear aerodynamics significantly effected pressure distributions and steady aeroelastic behavior in the transonic regime.

The present study expands upon the previous paper (Reference 5) by including the effects of a viscous boundary layer. Control surface reversal dynamic pressures are calculated for both viscous and inviscid analyses and the effects of including flow viscosity are considered.

Approach

Transonic Small Disturbance Theory

Because flow in the transonic region is affected by shocks, the analyses in this regime included the flow nonlinearities generated across the shocks. The method employed in this study was transonic small-disturbance (TSD) theory. Although one of the simplest forms of nonlinear aerodynamics, TSD theory is capable of determining the strength and location of weak shocks and because of its efficiency, is generally considered appropriate for preliminary design.

The aeroelastic calculations were performed by the NASA Langley code, CAP-TSD.[6] Using the finite-difference method, the program solves the general frequency modified transonic small disturbance potential equation, given here in differential form as

$$\frac{\partial f_0}{\partial t} + \frac{\partial f_1}{\partial x} + \frac{\partial f_2}{\partial y} + \frac{\partial f_3}{\partial z} = 0 \tag{1}$$

where

$$\begin{aligned} f_0 &= -A\phi_t - B\phi_x \\ f_1 &= E\phi_x + F\phi_x^2 + G\phi_y^2 \\ f_2 &= \phi_y + H\phi_x\phi_y \\ f_3 &= \phi_z \end{aligned} \tag{2}$$

The coefficients A, B, and E are defined as

$$A = M_\infty^2, \quad B = 2M_\infty^2, \quad E = 1 - M_\infty^2 \tag{3}$$

Within CAP-TSD there are a number of options for specifying the coefficients F, G, and H, depending upon the assumptions used in deriving the transonic small-disturbance equation. For the nonlinear analyses, the coefficients were

$$F = -\frac{1}{2}(\gamma+1)M_\infty^2, \quad G = -\frac{1}{2}(\gamma-3)M_\infty^2, \quad H = -M_\infty^2 \tag{4}$$

and for the linear cases

$$F = G = H = 0 \tag{5}$$

Viscous Effects

The effects of viscosity are included through the modeling of a viscous boundary layer that is

approximated by the turbulent boundary layer on a flat plate. Solution of the lag-entrainment boundary layer equations yields the momentum thickness, shape factor, and entrainment coefficient for the boundary layer as a function of distance along the chord.

Within CAP-TSD, the solution technique is based upon the implementation by Howlett of Interactive Boundary Layer Modeling.[7] IBLM treats the complete dynamic system as two coupled portions; the outer inviscid flow and the inner viscous flow. The amount of coupling error between the two systems is minimized as the edge velocities of the inner flow and outer flow regions are matched.

In general, both attached and separated boundary layer flow are treated through an inverse solution scheme which is necessary as the boundary layer equations become singular when the flow becomes separated.

It is beyond the scope of this work to fully describe the development of the viscous CAP-TSD code, CAP-TSDV, or the numerical solution of the boundary layer parameters. For further description of those matters, Reference 8 should be consulted.

Euler Computational Fluid Dynamics

In order to compare inviscid CAP-TSD results with a higher order computational fluid dynamics code, a number of Euler CFD runs were made utilizing the ENS3DAE (Euler/Navier Stokes Three-Dimensional Aeroelastic) CFD software. Like CAP-TSD, ENS3DAE is a tightly-coupled methodology for the computation of inviscid and viscous flows about flexible aircraft structures. The aerodynamic method is a central-difference, multi-block, approximate factorization algorithm for the implicit time integration of the Euler or Navier-Stokes equations, and is second-order accurate in both space and time. ENS3DAE has been extensively applied and modified since its delivery to Air Force Wright Laboratory (now Air Force Research Laboratory, Air Vehicles Directorate) by the then Lockheed Aeronautical Systems Company. Further details of the methodology, including applications to practical configurations, are provided in References 9-11.

For the ENS3DAE analysis of the thin wing in this study, a two-zone H-H grid topology is used. A planform view of the grid is shown in Figure 2. Each zone is comprised of 120 points in the streamwise direction, 50 points normal to the wing, and 59 spanwise points, leading to a complete grid of 708,000 points. On the wing surface, 61 points are distributed in the streamwise direction and 45 in the spanwise direction. Grid-point clustering is maintained along the flaperon hingeline and along the leading and trailing edges, similar to that employed for the Goland wing in Reference 3. Dimensions of the computational domain are identical to those specified for the CAP-TSD analysis. This aeroelastic definition has the advantage of providing structural modeling consistency between CAP-TSD and ENS3DAE.

Steady Aeroelastic Analysis

Aeroelastic analyses in CAP-TSD and ENS3DAE are carried out in generalized modal coordinates. Required mode shapes were obtained through an eigenvalue analysis in which the stiffness and mass of the system were represented by the finite element method. Structural eigenvalues, eigenvectors, and generalized mass and stiffness were determined using the Automated Structural Optimization System (ASTROS)[12]. The structural eigenvectors were then splined to the aerodynamic degrees of freedom, represented by the CAP-TSD or ENS3DAE computational mesh, using the infinite-plate spline[13]. With the splined mode shapes and generalized mass and stiffness, the static aeroelastic analysis was performed using appropriate boundary conditions in CAP-TSD or ENS3DAE. These analysis yielded the velocity potentials and pressure coefficients at the computational mesh nodes. Finally, the pressure coefficients were integrated to obtain the necessary aerodynamic coefficients and stability derivatives.

Since steady state roll performance was the subject of this study, a parameter used in the investigation of rolling maneuver performance was employed. Control surface effectiveness is defined as the flexible to rigid ratio of the rolling moment stability derivative produced by a control surface deflection at a given flight condition. Control surface effectiveness, ε, is given by the following

$$\varepsilon = \frac{C_{M_{\delta a_{flexible}}}}{C_{M_{\delta a_{rigid}}}} \qquad (6)$$

where the numerator and denominator are respectively the flexible and rigid derivatives of the rolling moment coefficients with respect to control surface deflection. Assuming a constant angle of attack and control surface deflection, the rigid rolling moment coefficient varies with Mach number only. For the aeroelastic condition, this coefficient varies with Mach number and dynamic pressure as structural flexibility is included in the analysis.

A steady aeroelastic phenomenon of interest, control surface reversal, occurs when ε becomes zero. Determination of control surface effectiveness at various

Mach numbers and dynamic pressures yields the control surface reversal points. A plot of ε against dynamic pressure gives the reversal point for a particular Mach number. This procedure is carried out for both viscous and inviscid analyses. Doing so allows the significance of the inclusion of viscous effects in the prediction of control surface effectiveness and reversal points to be quantified.

Analysis Model

This analysis procedure was carried out on a model of a generic fighter type aircraft, taken from Reference 14. The structural model of the wing was a fully built-up finite element model with a stiffness representative of stiff, low aspect ratio fighter wings. A NACA 0004 airfoil was used to represent the wing thickness. A single inboard trailing edge control surface, or flaperon was utilized. The full computational mesh for this model was a 154 x 46 x 80 grid. 100 chordwise and 23 spanwise grid points were used on the aerodynamic surface. The planform geometry and CAP-TSD aerodynamic mesh of this wing are depicted in Figure 1. The ENS3DAE Euler grid is shown in Figure 2, and the finite element model is shown in Figure 3.

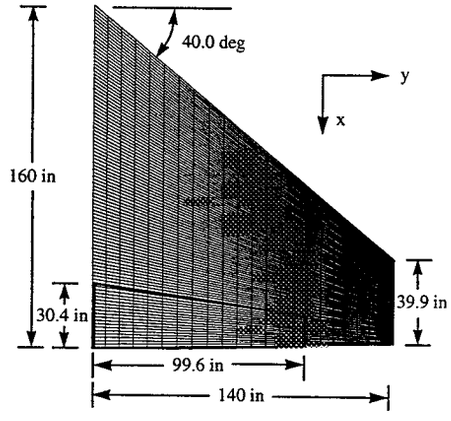

Figure 1: Fighter Wing Planform and CAP-TSD Small Disturbance Mesh

Rigid and flexible aeroelastic analyses were performed to obtain control surface effectiveness values using both nonlinear and linear aerodynamics. The boundary condition consisted of a cantilevered wing root, zero degree initial angle of attack, and one degree downward control surface rotation.

Plots of ε against dynamic pressure, q, were generated at Mach numbers from 0.70 to 0.97. All analyses were performed retaining a constant sea level density while matching velocity with dynamic pressure.

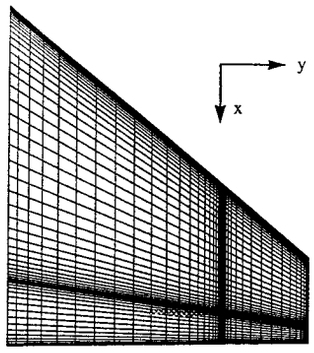

Figure 2: ENS3DA Euler Computational Mesh

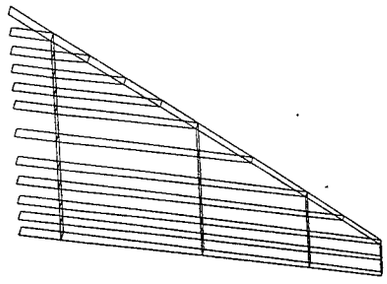

Figure 3: Fighter Wing Finite Element Model

Results

CAP-TSD Analyses

Three types of analyses were performed on the wing model. For baseline comparison, a linear inviscid analysis was performed. A nonlinear inviscid analysis was then performed to determine changes in pressure distribution due to nonlinear aerodynamics. Finally, a complete nonlinear viscous analysis was performed to observe the effects of the presence of a viscous boundary layer. These analyses were done over a range of Mach numbers varying from 0.70 to 0.97. Both rigid and flexible analyses were performed to illustrate the effects of structural flexibility in the transonic regime.

To gain a basic understanding of the aerodynamics associated with nonlinear and viscous effects without the influence of structural flexibility, rigid analyses were first performed and resultant pressure distributions were computed. Results for these analyses are shown in Figures 4 through 6 for Mach numbers of 0.70, 0.94, and 0.96. At Mach 0.70, as Figures 4a-4c illustrate, there were few qualitative differences among the results of the three analyses. As expected, no shocks developed on the wing at this subsonic Mach number, resulting in little difference between the linear inviscid and nonlinear inviscid analyses (Figs. 4a and 4b).

Results of the nonlinear inviscid and nonlinear viscous analyses are presented in Figures 4b and 4c. At

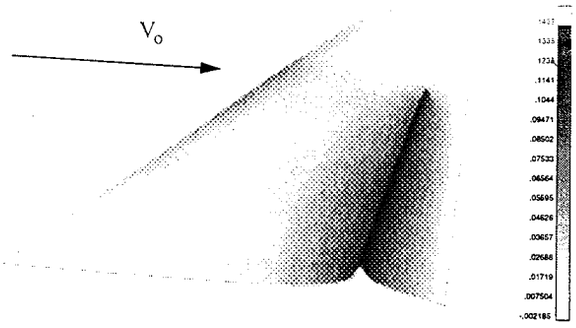

Figure 4a: CAP-TSD Rigid Linear Inviscid Resultant Pressure Distribution at Mach 0.70

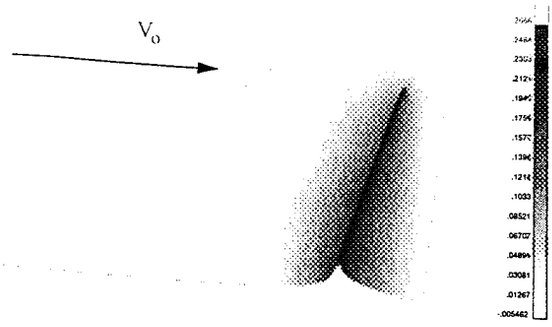

Figure 5a: CAP-TSD Rigid Linear Inviscid Resultant Pressure Distribution at Mach 0.94

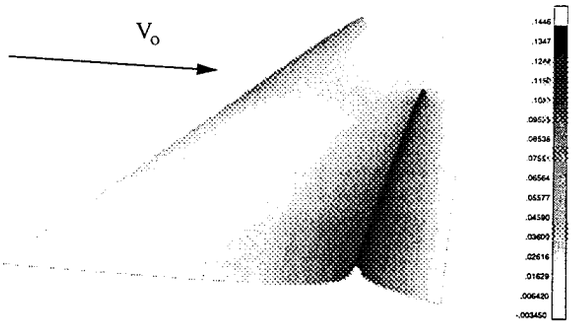

Figure 4b: CAP-TSD Rigid Nonlinear Inviscid Resultant Pressure Distribution at Mach 0.70

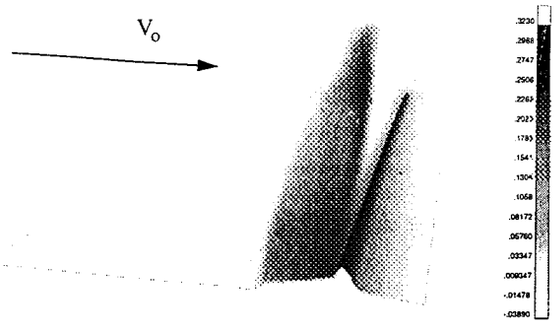

Figure 5b: CAP-TSD Rigid Nonlinear Inviscid Resultant Pressure Distribution at Mach 0.94

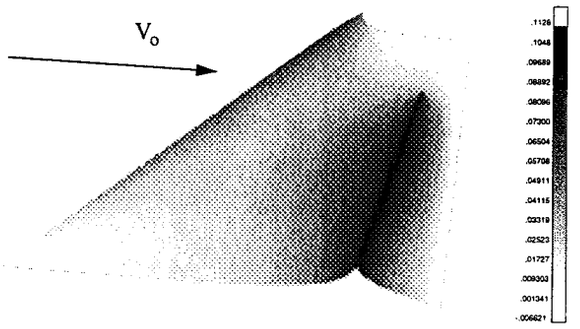

Figure 4c: CAP-TSD Rigid Nonlinear Viscous Resultant Pressure Distribution at Mach 0.70

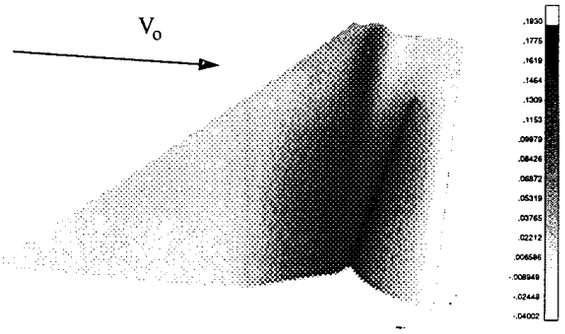

Figure 5c: CAP-TSD Rigid Nonlinear Viscous Resultant Pressure Distribution at Mach 0.94

this flow condition, qualitative differences between the two cases are again minor. Quantitatively, the effects of viscosity lead to a decrease in the magnitude of the pressure spike at the control surface hinge line.

Flow nonlinearities become significant at higher Mach numbers. This is illustrated at Mach 0.94 in Figures 5a through 5c. In the case of the linear analysis (Fig. 5a), the only pressure rise predicted is at the control surface hinge line. When nonlinear aerodynamics are included, however, a second pressure rise is generated (Fig. 5b). At this transonic Mach number, shocks form on the surface of the wing upstream of the control surface hinge line. Due to the deflection of the control surface, the positions of the shocks are altered so that the shock on the upper surface is further downstream than the shock on the lower surface. This results in a pressure rise in the chordwise region between the shocks as the higher pressure field on the lower surface is free to propagate further upstream than the pressure field on the upper surface.

At this transonic Mach number, the effects of viscosity are increased and result in a general chordwise

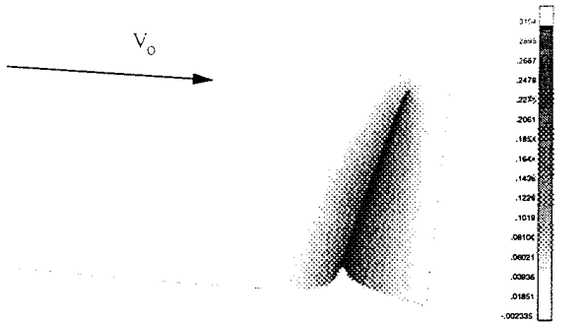

Figure 6a: CAP-TSD Rigid Linear Inviscid Resultant Pressure Distribution at Mach 0.96

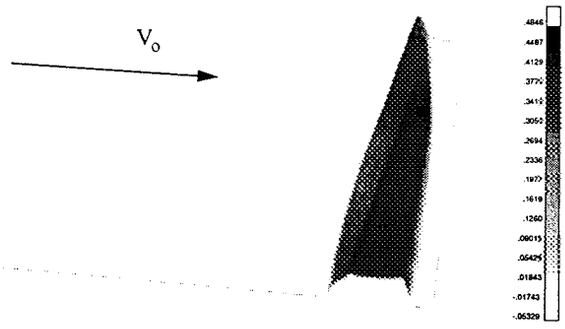

Figure 6b: CAP-TSD Rigid Nonlinear Inviscid Resultant Pressure Distribution at Mach 0.96

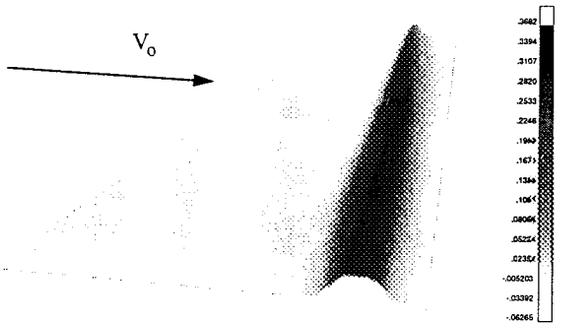

Figure 6c: CAP-TSD Rigid Nonlinear Viscous Resultant Pressure Distribution at Mach 0.96

smoothing of the pressure field (Fig. 5c). As with the case at Mach 0.70, the magnitude of the pressure spike at the hinge line is reduced. In this case, though, the difference is greater. Furthermore, the pressure rise in the region of the shocks is also reduced as viscous effects near the shocks are taken into account.

At a slightly higher Mach number of 0.96, the differences between the linear and nonlinear analyses remain significant (Figs. 6a and 6b). Again, shocks form on the surface of the wing and dramatically change the pressure field as aerodynamic nonlinearities are included. At this Mach number, the location of the

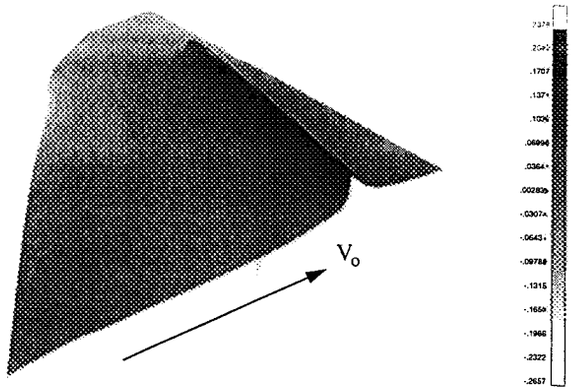

Figure 7a: CAP-TSD Aeroelastic Linear Inviscid Resultant Pressure Distribution at Mach 0.94

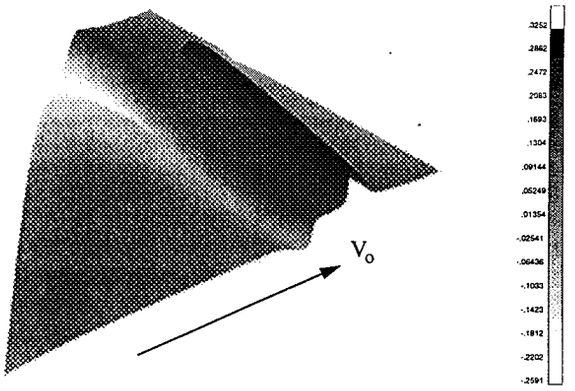

Figure 7b: CAP-TSD Aeroelastic Nonlinear Inviscid Resultant Pressure Distribution at Mach 0.94

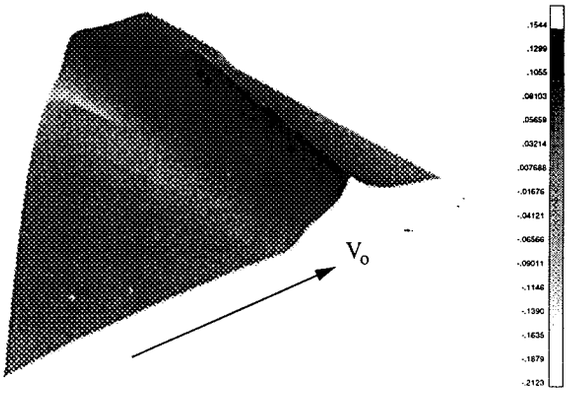

Figure 7c: CAP-TSD Aeroelastic Nonlinear Viscous Resultant Pressure Distribution at Mach 0.94

shocks are shifted downstream and the shock on the upper surface now falls aft of the control surface hinge line.

When viscous effects are included (Fig. 6c), the effects are even more significant than those seen at the previous Mach numbers. As with the prior cases, the

general trend is a lowering of the magnitude of the pressure rises in the region of the shocks and at the control surface hinge line. The smoothing of the pressure field is significant and results in lower chordwise pressure gradients than predicted by the inviscid analysis.

Structural flexibility was included in the analyses at Mach 0.94. The resultant pressure coefficient distributions are shown in Figure 7a through 7c. The consequences of a flexible structure become evident as the leading edge of the wing twists downward in response to the pressure rises aft of the structural elastic axis. This leads to negative resultant pressures near the leading edge, and at a certain dynamic pressure, results in control surface reversal, or the point at which a control surface is completely ineffective at generating a rolling moment.

For the linear inviscid case, the only adverse twisting of the wing is due to the pressure rise at the control surface hinge line (Fig. 7a). In the nonlinear case, there is a second contribution due to the pressure rise in the region of the shocks as seen in Figure 7b. This leads to a greater twisting of wing, and consequently, lower reversal dynamic pressures.

Inclusion of viscous effects (Fig. 7c), as seen in the rigid analyses, leads to a general reduction in the magnitude of pressure rises. This effectively lessens the moment acting to twist the wing. As a result, inclusion of viscosity in this study generated higher reversal dynamic pressures than predicted by an inviscid analysis.

Comparison of TSD and Euler Analyses

An important aspect of this work is the determination of the adequacy of transonic small disturbance theory in predicting the pressure distribution on a lifting surface with a deflected control surface in transonic flow. To gain some insight into this issue, a number of ENS3DAE analyses were made so that the CAP-TSD results could be compared against the higher-order results generated by Euler CFD.

The first of these comparisons is presented in Figure 8. The plot shows a chordwise pressure distribution predicted by CAP-TSD and ENS3DAE for the rigid case at a subsonic Mach number of 0.70 and a low transonic Mach number of 0.93. The spanwise station is at approximately the mid-span of the control surface. To obtain a baseline comparison, the control surface was not deflected. At this symmetric condition, the upper and lower surface pressure coefficients collapse to the same values. The results generated by the two codes are in close agreement.

The next comparison concerned the agreement of

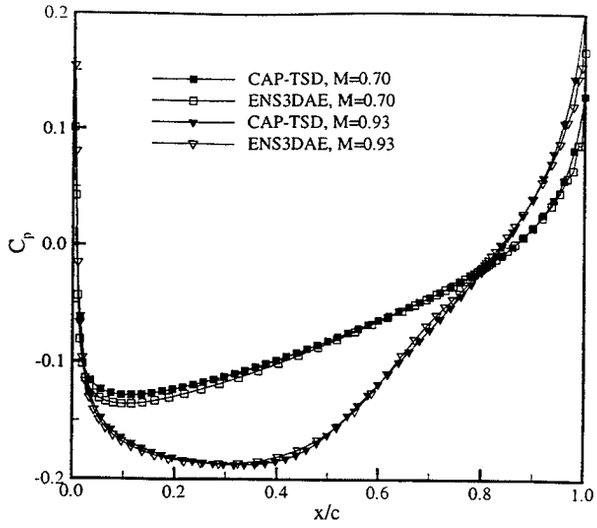

Figure 8: Chordwise Rigid Pressure Distribution for No Control Surface Deflection

the prediction of the pressures generated at the control surface hinge line due to a one degree downward control surface deflection. The results for a rigid subsonic analysis at Mach 0.70 are shown in Figure 9. Again, the predicted pressure distributions are in close agreement for both upper and lower surfaces. ENS3DAE predicts slightly larger pressure changes at the hinge line because the chordwise spacing of the Euler grid is finer at this location than the CAP-TSD grid. The rolling moment coefficients are in agreement within 15 percent with a value of 0.0127 predicted by CAP-TSD and 0.0108 by ENS3DAE.

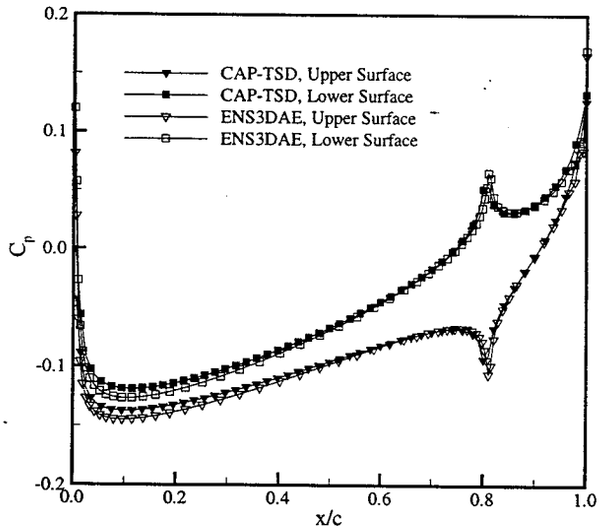

Figure 9: Chordwise Rigid Pressure Distribution for 1 Degree Control Surface Deflection at M=0.70

The same analysis for a one degree control surface deflection was performed at a Mach number of 0.94. The upper and lower surface pressure coefficients for this case are plotted in Figure 10. At this transonic Mach number, there is a clear discrepancy between the CAP-TSD and ENS3DAE results in the prediction of the strength and location of the shocks on the surface of the wing. This results in a significant difference in the calculated rigid rolling moment coefficient. CAP-TSD yielded a value of 0.0200 while ENS3DAE predicted a value of 0.0157. The difference in shock location and strength remains significant for the flexible condition as shown in Figure 11.

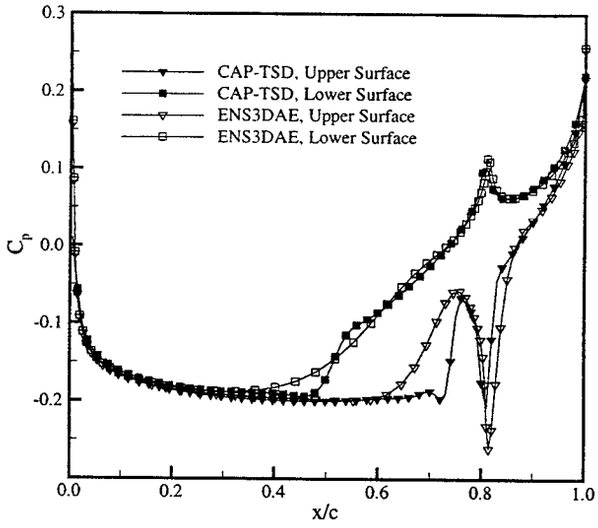

Figure 10: Chordwise Rigid Pressure Distribution for 1 Degree Control Surface Deflection at M=0.94.

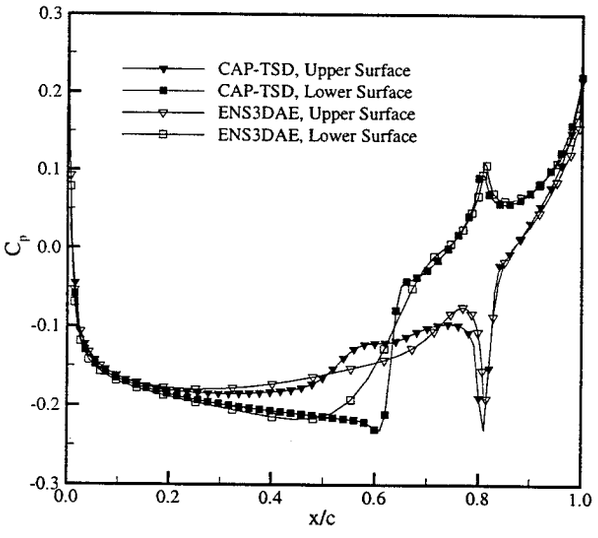

Figure 11: Chordwise Aeroelastic Pressure Distribution for 1 Degree Control Surface Deflection at M=0.94.

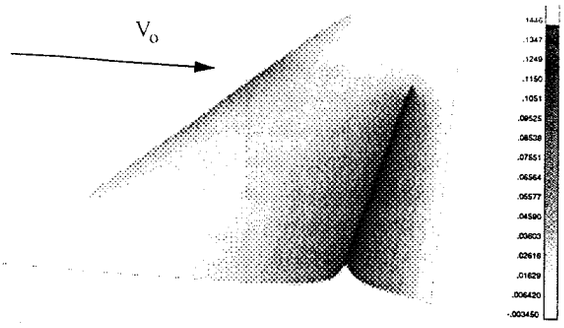

Figure 12a: CAP-TSD Resultant Pressure Distribution at Mach 0.70

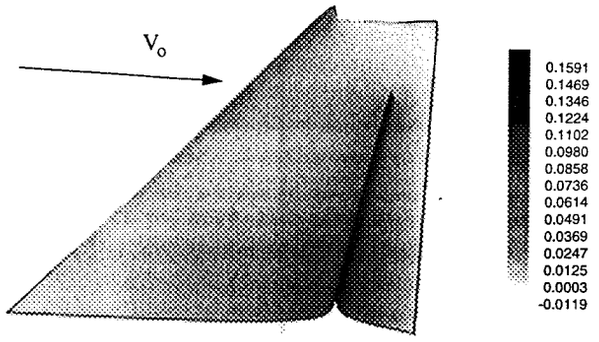

Figure 12b: ENS3DAE Resultant Rigid Pressure Distribution at Mach 0.70

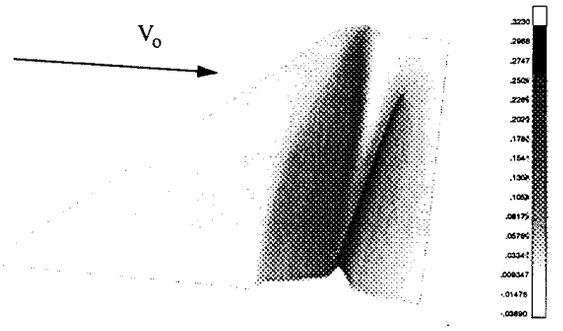

Figure 13a: CAP-TSD Resultant Rigid Pressure Distribution at Mach 0.94

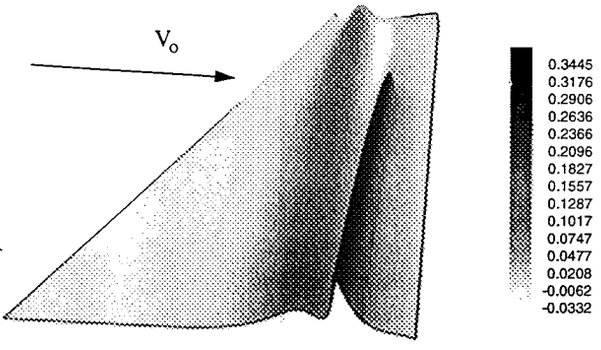

Figure 13b: ENS3DAE Resultant Rigid Pressure Distribution at Mach 0.94

To obtain a clearer qualitative comparison between CAP-TSD and ENS3DAE results, three dimensional carpet plots of the pressure distribution due to a one degree control surface deflection were generated for the rigid case using both codes. The results at Mach 0.70 are shown in Figure 12a-b. The corresponding results for Mach 0.94 are illustrated in Figures 13a-b. As seen in the previous chordwise pressure plots, the results from the codes agree well for the subsonic case. At the transonic Mach number, however, a difference in the pressure rise in the region of the shocks is apparent.

The influence of aerodynamic nonlinearities and flow viscosity on the variation of reversal dynamic pressure with Mach number is shown in Figure 14. In addition to trend results generated by CAP-TSD, a single reversal point at Mach 0.94 was calculated using ENS3DAE. Consistent with the observations made from the resultant pressure distributions predicted by CAP-TSD, the nonlinear inviscid reversal dynamic pressures are lower than the linear inviscid reversal pressures. The nonlinear viscous reversal dynamic pressures are approximately ten percent higher than the nonlinear inviscid results, and are in fact higher than the linear inviscid reversal pressures except at Mach numbers beyond 0.96. The reversal point computed by ENS3DAE lies approximately ten percent higher than the corresponding CAP-TSD nonlinear inviscid analysis.

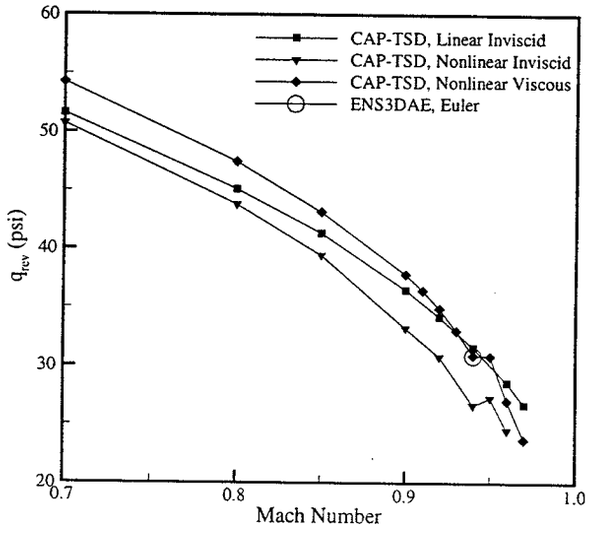

Figure 14: Control Surface Reversal Dynamic Pressures

Conclusions

The aeroelastic analyses of the wing model demonstrates that the presence of viscosity has an impact on the steady aeroelastic characteristics of the wing. Examination of pressure distributions indicates that viscous effects reduce the magnitude of the resultant pressure rises in the region of the wing aft of the structural elastic axis. This serves to delay control surface reversal and increases the dynamic pressure at which this aeroelastic phenomena occurs.

Since the overall objective of this research is to develop analysis techniques suitable for preliminary design of aircraft structures, the findings of this research should be viewed in this context. The results of this study indicate that it would not necessarily be beneficial to use a viscous analysis over the entire transonic regime to determine structural loadings for design purposes. As in the case considered in this work, use of the nonlinear inviscid results would result in a more conservative design without resorting to expensive viscous analyses.

It should be noted, however, that the results of this research are considered preliminary and by no means exhaustive. During this study, separated flow was not encountered; therefore no observations can yet be made concerning the impact of separated flow on reversal dynamic pressure. Furthermore, the upper Mach number explored was 0.97. Beyond this, stable solutions were not obtained. Until a more complete picture of the reversal behavior in the complete transonic regime can be completed, it would be premature to suggest that viscous effects need never be accounted for in the preliminary design of aircraft structures subject to transonic flow conditions.

Comparisons between CAP-TSD and ENS3DAE Euler analyses showed some differences in the predicted pressure coefficient distributions, most notably at transonic conditions where the deflection of a control surface modifies the characteristics of the shocks on the surface of the wing. Further ENS3DAE comparisons should be made to determine if this difference can be accounted for through mesh refinement since the CAP-TSD mesh was considerably finer in the chordwise direction. If the differences cannot be resolved, the adequacy of transonic small disturbance theory in these types of analyses should be considered.

To gain a more complete understanding of the influence of viscosity on steady aeroelastic phenomena, further research needs to be conducted. As already stated, effects of viscosity should be explored over the complete transonic regime. Separated flow, particularly at the base of the shocks should also be investigated. Navier-Stokes CFD analyses should be made in ENS3DAE to correlate the effects of viscosity predicted with this higher order scheme to those obtained from transonic small disturbance theory with boundary layer corrections.

Finally, stability issues at Mach numbers where shocks are located at the trailing edge of the wing call

into question the adequacy of transonic small disturbance theory at this flow condition. At the least, results obtained from TSD theory should be compared against results obtained from the higher order CFD codes before a technique involving TSD theory is incorporated into the preliminary design environment.

Acknowledgments

The authors wish to recognize Major Brian Sanders of the Air Force Office of Scientific Research. Major Sanders is responsible for the funding support of this research.

The authors also wish to acknowledge the Major Shared Resource Centers at Aeronautical Systems Center, Wright Patterson Air Force Base, OH, and Army Research Lab located at Aberdeen Proving Ground, MD. These high performance computing centers provided the computational hardware used in this research.

References

[1]Sotamayer, W.A., "Unsteady Transonic Flow for a Wing with Control Surface Deflections," AFWAL TM-86-186-FIBR, January 1987.

[2]Bharadvaj, B.K., "Computation of Steady and Unsteady Control Surface Loads in Transonic Flow," AIAA Paper 90-0935-CP, April 1990.

[3]Miller, G.D., "Active Flexible Wing (AFW) Technology," AFWAL TR-87-3096, February 1988.

[4]Pitt, D.M., and Fuglsang, D.F., "Aeroelastic Calculations for Fighter Aircraft Using the Transonic Small Disturbance Equation," Paper No. 16, AGARD CP 507, Presented at the 73rd meeting of the AGARD Structures and Materials Panel, San Diego, CA, Oct 7-11 1991.

[5]Andersen, G.R., Kolonay, R.M., and Eastep, F.E. "Control Surface Reversal in the Transonic Regime", AIAA Paper 97-1385-CP, Presented at the AIAA Structures, Structural Dynamics, and Materials Conference, Kissimmee, FL, April 1997.

[6]Batina, J.T., "A Finite-Difference Approximate-Factorization Algorithm for Solution of the Unsteady Transonic Small-Disturbance Equation," NASA Technical Paper 3129, January 1992.

[7]Howlett, J.T., "Efficient Self-Consistent Viscous Inviscid Solution for Unsteady Transonic Flow," Journal of Aircraft, Vol. 24, Nov. 1987, pp. 737-744.

[8]Edwards, J.W., "Transonic Shock Oscillations and Wing Flutter Calculated with an Interactive boundary Layer Coupling Method," Presented at EUROMECH-Colloquium 349 Simulation of Fluid-Structure Interaction in Aeronautics, Göttingen, Germany, Sept. 16-18, 1996

[9]Schuster, D.M, Vadyak, J., and Atta, E., "Static Aeroelastic Analysis of Fighter Aircraft Using a Three-Dimensional Navier-Stokes Algorithm," Journal of Aircraft, Vol. 27, No. 9, Sept., 1990, pp. 820-825.

[10]Schuster, D.M., "Application of Navier-Stokes Aeroelastic Methods to Improve Fighter Wing Performance," Journal of Aircraft, Vol. 32, No. 1, Jan.-Feb., 1995, pp. 77-83.

[11]Schuster, D.M., Beran, P.S., and Huttsell, L.J., "Application of the ENS3DAE Euler/Navier-Stokes Aeroelastic Method," Proceedings of the AGARD 85th Structures and Materials Panel Workshop on Numerical Unsteady Aerodynamic and Aeroelastic Simulation, Aalborg, Denmark, October 14-15, 1997, pp. 11.

[12]Johnson, E.H., and Venkayya, V.B., "Automated Structural Optimization System (ASTROS)," Vol. I, Theoretical Manual, AFWAL TR-88-3028, December 1988.

[13]Harter, R.L., and Desmarais, R.N., "Interpolation Using Surface Splines," Journal of Aircraft, Vol. 9, No. 2, February 1972.

[14]Canfield, R.A., and Jacques, D., "Effect of Modal Sensitivity on Flutter Eigenvalue Derivatives", AIAA Paper 94-1545.